Absolute measurement of the Fano factor using a Skipper-CCD

Dario Rodrigues,[1,2] Kevin Andersson,[1,2] Mariano Cababie,[1,2] Andre Donadon,[1,2] Gustavo Cancelo,[2] Juan Estrada,[2] Guillermo Fernandez-Moroni,[2] Ricardo Piegaia,[1] Matias Senger,[1,2] Miguel Sofo Haro,[2,3] Leandro Stefanazzi,[2] Javier Tiffenberg,[2] and Sho Uemura[4]

[1)]*Department of Physics, FCEN, University of Buenos Aires and IFIBA, CONICET, Buenos Aires, Argentina*

[2)]*Fermi National Accelerator Laboratory, PO Box 500, Batavia IL, 60510*

[3)]*Centro Atómico Bariloche, CNEA/CONICET/IB, Bariloche, Argentina*

[4)]*Raymond and Beverly Sackler School of Physics and Astronomy, Tel-Aviv University, Tel-Aviv 69978, Israel*

(Dated: 27 April 2020)

Skipper-CCD can achieve deep sub-electron readout noise making possible the absolute determination of the exact number of ionized electrons in a large range, from 0 to above 1900 electrons. In this work we present a novel technique that exploits this unique capability to allow self-calibration and the ultimate determination of silicon properties. We performed an absolute measurement of the variance and the mean number of the charge distribution produced by ^{55}Fe X-rays, getting a Fano factor absolute measurement in Si at 123K and 5.9 keV. A value of 0.119 ± 0.002 was found and the electron-hole pair creation energy was determined to be (3.749 ± 0.001) eV. This technology opens the opportunity for direct measurements of the Fano factor at low energies.

I. INTRODUCTION

The ratio between the observed statistical fluctuations in the number of charge carriers and that expected from a pure Poisson statistics, the Fano[1] factor F, has been historically used –along with the electron-hole pair creation energy ε_{eh} to characterize the response of different detectors to X radiation[2–6].

A precise determination of ε_{eh} has also implications for Dark Matter Searches[7] and reactor-Neutrino experiments[8] to reconstruct the energy deposited by interacting particles in the detector. To measure F at low energies is also key in the sensitivity calculation of low-mass dark matter experiments[9,10]. For a review of ionization modeling in silicon at low energy and further discussion of ε_{eh} and F see Ref. 11.

Additionally, both ε_{eh} and F have a significant role in the calibration requirements of Charge Coupled Devices (CCD) imaging spectrometers, such as in astronomy[12], and have been measured in Si using conventional CCDs[13–16]. Since these kind of measurements are affected by sensor calibration accuracy, different approaches were proposed to reduce the contribution from systematic uncertainties in gain determination. For instance, Kotov et al.[16] have used an optical technique which takes advantage of the Poisson distribution properties.

One of the main contributions to systematic uncertainty when using a conventional CCD comes from the low-frequency noise (σ_{RN}), which impose a lower limit to the readout noise of nearly $\sigma_{RN} \approx 1.8$ e$^-$ rms/pix[15,17]. As a consequence, the actual variance of the charge distribution (σ^2) cannot be measured, and instead, a larger $\sigma^2_{obs} = \sigma^2 + \sigma^2_{RN}$ is observed. Such readout noise essentially makes the direct determination of F impossible for low energies where σ^2_{RN} cannot be neglected against σ^2. Furthermore, the capability to reconstruct the total charge produced by each event is also affected by charge collection inefficiencies, and the difficulty to determine the actual size of each cluster of pixels produced by each interaction, which introduce an extra systematic uncertainties.

TABLE I. Main characteristics of the CCD detector used in this work.

Characteristics	Value	Unit
Format	4126 x 886	pixels
Pixel size	15	um
Thickness	200	um
Operating Temperature	123	K
Readout noise (1 sample)	3.5	e$^-$ rms/pix
Readout noise (300 samples)	0.20	e$^-$ rms/pix

Here we report the first measurement of ε_{eh} and F using a Skipper-CCD, which allows to reach sub-electron readout by measuring the charge in each pixel as many times as desired without destroying it. Exploiting this feature, we developed a novel method for absolute self-calibration by identifying the quantized-charge peaks that correspond to all electron multiplicities between 0 and $\sim$1900 e$^-$. Based on this, taking advantage of the almost perfect Charge Collection Efficiency (CCE) and the sub-electron readout noise, our results represent the most precise measurement of both ε_{eh} and F in Si.

II. SKIPPER-CCD DETECTOR

The main difference between conventional scientific CCDs and Skipper-CCDs lies in the non-destructive readout system of the latter, which allows to repeatedly measure the charge in each pixel. For uncorrelated samples, this capability results in the reduction of the readout noise in a factor equal to the square root of the number of samples[18]. This feature enables the precise determination of the number of electrons in each pixel, which means that single photon counting is possible in the low energy region (optical and near-infrared).

Table I describes the main characteristics of the back-illuminated fully-depleted CCD used in this work. The detector is divided in four quadrants, each of them constituted

This manuscript has been authored by Fermi Research Alliance, LLC under Contract No. DE-AC02-07CH11359 with the U.S. Department of Energy, Office of Science, Office of High Energy Physics.

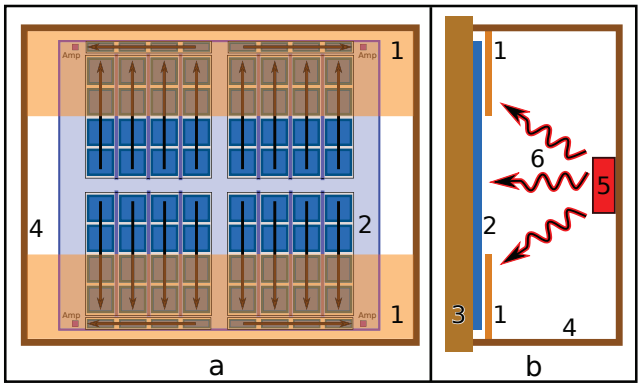

FIG. 1. Experimental setup. a) Front view. b) Lateral view. Arrows indicate how the charges are moved in each quadrant during readout. 1: Thin Cu foils cover half of the detector near amplifiers to shield them from direct X-ray illumination. 2: Skipper-CCD, 3: Cold Cu piece, 4: Cold Cu box, 5: ^{55}Fe radioactive source, 6: X-rays.

by 443 rows and 2063 column. The general structure of the detector pixel array is schematized in Fig. 1a.

By contrast to others scientific CCD with several microns of dead layer in the back, the Skipper-CCD used in this work has a special back side treatment for photon collection[19]. That side is covered by three thin layers: ∼20 nm Indium Tin Oxide (ITO), ∼38 nm ZrO_2, and ∼100 nm SiO_2. The detector was installed in a 30 cm × 30 cm × 30 cm aluminum Dewar and it was cooled at 123K using a cryocooler. The readout and control systems are fully integrated in a new single-board electronics optimized for Skipper-CCD sensors. This Low-Threshold-Acquisition system (LTA) was developed in-house[20] and provides a flexible and scalable solution for detectors with target masses up to a few hundred grams.

III. CALIBRATION AND LINEARITY

A self-calibration procedure was performed to determine the relationship between the number of electrons in each pixel and the signal readout value in Analog to Digital Units (ADU). An LED installed inside the Dewar was used to populate the CCD pixels with the electrons produced by 405 nm photons. In order to cover a large range of electrons per pixel, we performed several measurements increasing the light exposure time. Thus, we produced different overlapping Poissonian distributions with increasing mean number of electrons. All these measurements were performed taking 300 samples per pixel. As a result, the readout noise was reduced by a factor $\sqrt{300} \sim 17.3$, achieving a final value of 0.2 e$^-$. This allowed us to distinguish between consecutive peaks in the full range from zero up to 1900 e$^-$. The mean value in ADU for each of those peaks was determined by means of Gaussian fits. Then, we completed the self-calibration by simple assignment of each ADU mean value to the corresponding peak number, *i.e.* the number of electrons. Fig. 2 presents the peaks in the region between 1560 and 1582 electrons.

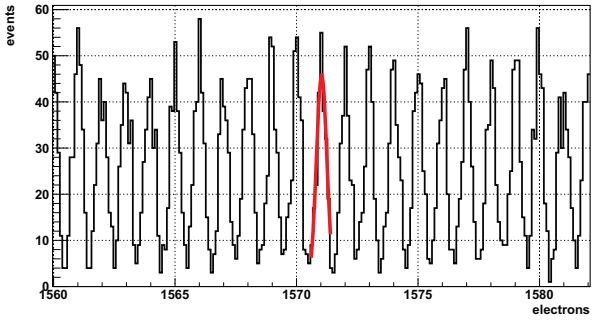

FIG. 2. Self-calibration performed taking 300 samples per pixel. The ADU mean numbers per peak where fitted against the peak number using a fourth-degree polynomial to take into account for nonlinearities. Here we display a zoom of the full spectrum centered at the electron mean number produced by 5.9 keV X-rays peaks from ^{55}Fe. All the peaks from 0 to ∼1900 e$^-$ are clearly identified in the full spectrum.

In regards to the nonlinearities in the amplifier, Fig. 3 displays departures from 1 of the ratio between the number of electrons calculated from a linear self-calibration and the actual number of electrons per pixel. In contrast with the usual nonlinearity measurements in conventional CCD amplifiers (see, for instance, Fig. 1 in Ref. 21), Skipper-CCDs allow to quantify nonlinearities for all occupancies in a full range.

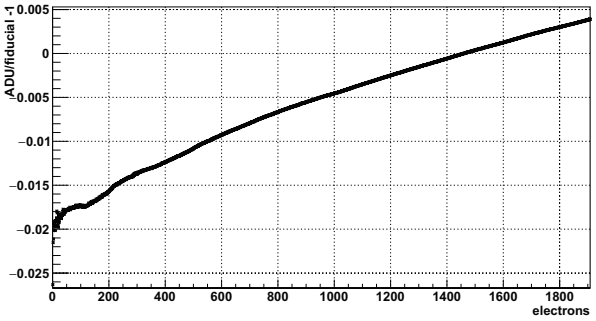

FIG. 3. Nonlinearities in one of the four Skipper-CCD amplifiers. The *y* axis plots the fractional change in the number of electrons from calibration relative to the actual one, perfectly linear amplifier would yield zeros.

IV. MEASUREMENTS

The X_K rays emitted after the ^{55}Fe electron capture decays are widely used for CCD calibration[15]. Their energies, known with excellent precision, are summarized in Table II. For our purpose, we used an electroplated ^{55}Fe radioactive source with a diameter of ∼5 mm and an activity of ∼0.1 μCi. This source was placed facing the backside of the CCD and ∼40 mm apart as depicted in Fig. 1b.

TABLE II. ^{55}Fe X-rays energies and Intensities of interest in this work. Source: https://xdb.lbl.gov/

X_K	Energy (keV)	Rel Intensity
α_2	5887.6	8.5 (4)
α_1	5898.8	16.9 (8)
β_3	6490.4	3.4 (8)

In a significant fraction of the ^{55}Fe decays, the energy is transferred to an orbital electron instead of an X-ray. These Auger electrons leave the atom with an energy just a few eV lower than the X-rays due to the ionization energy, and create a continuous energy spectrum when they hit the CCD. To avoid this background we covered the ^{55}Fe source with a 20 μm Mylar foil that stops the keV-electrons and has very small probability of producing small-angle Compton scattering of the X-rays.

a. Data acquisition procedure To reduce impact of dark current we limit the exposure/readout time by simultaneously reading the 4 quadrants of the CCD and restricting the acquisition to only 50 rows per quadrant. Each row containing 500 pixels (7 prescan, 443 active, and 50 overscan) at 300 samples per pixel. This corresponds to a readout time of $\sim$10 minutes per image. After readout, the 300 samples taken for each pixel are averaged and the empty pixels in the overscan are used to compute and substract a baseline for each row. The resulting image contains 443x50 pixels for each quadrant and the measured charge is represented in ADUs that is converted into electrons using the self-calibration procedure described above.

At the end of each exposure/readout cycle, all the charge collected by the CCD during this time is flushed in a quick clean procedure that takes about a second.

Because of the relatively high rate of X-rays photons hitting the CCD, we covered half of each quadrant with a thin Cu foil in the region close to the amplifiers (see Fig. 1). In this way, we exposed the uncovered area to the X-rays and then, we quickly move the charge collected in the exposed region of the CCD under the Cu foils where they wait to be read while they are shielded from the source.

b. Black body radiation shield To minimize backgrounds produced by infra-red (IR) photons emitted by the inner surfaces of the vacuum vessel, which is at room temperature, we covered the detector with a cold copper box as shown in Fig. 1b. This box is in thermal contact with the cold copper piece in which the detector is mounted and shields it from black body radiation originating on the surrounding walls.

V. DATA ANALYSIS AND RESULTS

a. Event reconstruction The images recorded using the procedure described above contain ionization events produced by X-rays from the ^{55}Fe source and other environmental radiation. A fraction of a typical image is presented in Fig. 4. As the Skipper-CCD used for this work was back-illuminated by the X-rays from the source, the resulting interactions mostly took place in the first 30 μm of the back-side of the CCD. Due to charge diffusion during the charge collection process, the charge of the resulting events is distributed among several pixels following a 2D Gaussian distribution[22]. The total number of electrons generated by each X-ray event was reconstructed by running a clustering algorithm in which all non-empty neighboring pixels are group together and are considered to be part of a the same event.

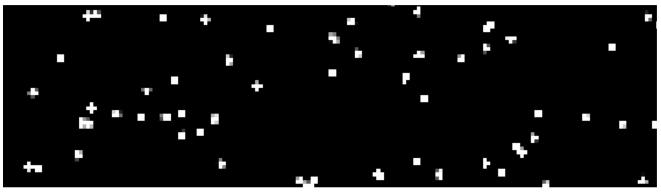

FIG. 4. Section of a Skipper-CCD image after exposing it to the X-rays emitted by the ^{55}Fe radioactive source where different cluster size can be identified.

It is worth noting that Skipper-CCD enables the charge determination in clusters of different sizes, introducing a negligible uncertainty in the estimation of the total number of electrons produced by each event. With a readout noise of 0.2 e^-, the boundaries of each cluster can be determined with a probability of miss classification as low as $p = 0.062$ per external surrounding pixel, which translates to an error lower than 0.05 e^- per cluster in average. In addition, this also implies that this measurement is robust to charge transfer inefficiencies that may spread the charge among neighboring pixels. The probability of any electron from an event being separated from the other electrons by one or more empty pixels is essentially null for all practical purposes.

b. Quality cuts To reject merged events, clusters with relatively large or small variance in any of both x and y directions were discarded and only relatively circular clusters, compatible with the expected 2D Gaussian shape[22], are selected. To reject Compton events produced in the bulk of the CCD by high-energy environmental radiation we place a cut on the size of the clusters to select events produced by interactions in the first 30 μm of the backside of the CCD. The clusters size distribution after these cuts has a mean value of (12.4 ± 2.7) pixels.

c. Readout noise The probabilities of counting one more and one less electron (with respect to the actual number) in the pixels building clusters are equal to p. Taking into account the cluster size distribution, eventual inner or external miss classification introduces a bias as low as 0.1 e^- and a readout noise $\sigma_{RN} = 0.5$ e^- rms/cluster. As will be seen soon, such a value of σ^2_{RN} can be safely neglected against σ^2.

d. Dark Current Effect The Dark Current (DC) was measured at the same experimental conditions but without the ^{55}Fe radioactive source. It was computed as the ratio between 1-electron events and empty pixels, resulting in $\sim 1\times10^{-5}$ electron per pixel per second.

Thus, taking into account the mean size of clusters, we expect only (0.04 ± 0.01) extra electrons due to the DC during the 10 minutes spent in exposing and reading each image. Therefore, the DC effect can be neglected without introducing

a significant bias in our results.

e. Charge Collection Efficiency There are two effects responsible for degrading CCE: recombination and charge transfer inefficiencies. As already discussed, the latter is insignificant when using Skipper-CCD. The cryogenic temperature of operation, the very low-doped silicon and the high electric field (∼350 V/mm) in the bulk of the CCD prevent signal charge to be lost by recombination. Furthermore, the total thickness of dead layers in our detector is less than 0.2μm, much smaller than the attenuation length of ∼6 keV photons in Si (∼25 μm). Therefore, the probability for such photons to interact with those layers is completely negligible. As a result, CCE in our detector can be considered essentially as one for all practical purposes.

f. Unbinned multipeaks fit K_α and K_β X-rays peaks were fitted using the likelihood given by Eq. (1). It is the result of the convolution of two exponential with one Gaussian distribution for each of the three peaks given in Table II (for a detailed derivation see Ref. 23).

$$\mathscr{L}(e|\mu_1,\mu_3,\sigma_1,\lambda_1,\lambda_2,\eta_1=\eta_2,\eta_3)=\sum_{j=1}^{3}I_j\left[\eta_j\frac{\lambda_1}{2}\exp\left[(e-\mu_j)\lambda_1+\frac{\sigma_j^2\lambda_1^2}{2}\right]\times\mathrm{Erfc}\left[\frac{1}{\sqrt{2}}\left(\frac{e-\mu_j}{\sigma_j}+\sigma_j\lambda_1\right)\right]+\right.$$
$$\left.(1-\eta_j)\frac{\lambda_2}{2}\exp\left[(e-\mu_j)\lambda_2+\frac{\sigma_j^2\lambda_2^2}{2}\right]\times\mathrm{Erfc}\left[\frac{1}{\sqrt{2}}\left(\frac{e-\mu_j}{\sigma_j}+\sigma_j\lambda_2\right)\right]\right] \quad (1)$$

where μ_j, σ_j and I_j represent the mean number, the standard deviation, and the relative intensity of each peak j with energy E_j. λ_1 and λ_2 stand for the parameters of the two exponential distributions convoluted with each Gaussian, while η_j sets the relative weight between those exponential.

Since the difference between the energy of K_α peaks is only 11.1 eV (see Table II), we can safely assume the same ε_{eh} and F for both of them. Therefore, we set $\mu_2=\mu_1\times E_2/E_1$ and $\sigma_2=\sigma_1\times\sqrt{E_2/E_1}$. In the case of K_β peak, we also assume the same F but we allowed for ε_{eh} to take a different value. These conditions are fulfilled by letting μ_3 be a free parameter (see Eq. (1)), and fixing $\sigma_3=\sigma_1\times\sqrt{\mu_3/\mu_1}$.

Fig. 5 presents the unbinned likelihood fit for the X-rays peaks over a total of 18085 events after selection and quality cuts. The relevant fitted parameters and the values for ε_{eh} and F are listed in Table III.

The fitted values for μ_1, μ_3 and σ_1 are very robust against changes in the energy range considered for fitting and therefore, so are the computed for ε_{eh} and F. Such changes only affect λ_1, λ_2, and η_j values, which essentially fulfill the function of modeling the effects of energy absorption in the Mylar foil (left tails in Fig. 5).

VI. DISCUSSION AND CONCLUSIONS

Our results are in agreement with two pioneer works: Ryan et al.[2], who almost fifty years ago have reported $\varepsilon_{eh}=3.745\pm0.003$ eV, and Alig et. al.[3], who almost forty years ago using Monte Carlo simulations found $F=0.113\pm0.005$. However, going to more recent works, we have found large discrepancies with other published results[12–14], where F values between 0.14 and 0.16 have been informed.

Although initially ε_{eh} and F were treated as material constants[2,3], since then, many authors have investigated experimentally[4–6,24] and by means of Monte Carlo simulations[12,25,26] their dependence on both energy and temperature. As a result, nowadays we know that, ε_{eh} decreases as the temperature or the energy increases, while F changes in a lesser extent.

Kotov et al.[16], using conventional CCD at 180K have reported ε_{eh}=(3.650 ± 0.009) eV and F=0.128 ± 0.001, however, according to the gradient informed by Lowe et al.[6], the difference with our results can not be explained as a consequence of the difference in temperature. We do observe a perfect agreement with the values published by Lowe et al.[6]. They have measured ε_{eh} as a function of temperature, and according to what they have reported, ε_{eh} =(3.743 ± 0.090) eV and F = 0.118 ± 0.004 is what we should expect at 123K.

We've shown how the sub-electron readout noise achieved by Skipper-CCDs enables its self-calibration. It allowed us to perform an absolute determination of the variance and mean number of the charge distribution produced by X-rays from ^{55}Fe. Thus, we've obtained the first Fano factor absolute measurement in Si and the most precise determination of both the electron-hole pair creation energy ε_{eh} and F.

A notable feature of our results is that thanks to the Skipper-CCD performance they were possible with neither subtracting reading noise nor correcting for CCE, as it was needed in previous work.

Ongoing experiments using X-rays from Al and F fluorescence will exploit the capability of this technology for probing the theoretically expected Fano factor at very low energies. Also, we are in the process of measuring ε_{eh} and F at different temperatures to experimentally observe the temperature dependence of these quantities.

ACKNOWLEDGMENTS

This work was supported by Fermilab under DOE Contract No. DE-AC02-07CH11359. This manuscript has been authored by Fermi Research Alliance, LLC under Contract

TABLE III. Fitted parameters obtained by maximizing the Likelihood given by Eq.(1). Fano factor was set to be the same for all peaks. ε_{eh} was set to be the same for α peaks. The result fitting only the β peak is also included.

X_K	μ	$\Delta\mu$	σ	$\Delta\sigma$	F	ΔF	ε_{eh}	$\Delta\varepsilon_{eh}$
α_2	1570.50	0.18	13.68	0.12				
α_1	1573.48	0.18	13.69	0.12	0.119	0.002	3.749	0.001
β_3	1730.50	0.55	14.36	0.13			3.751	0.002

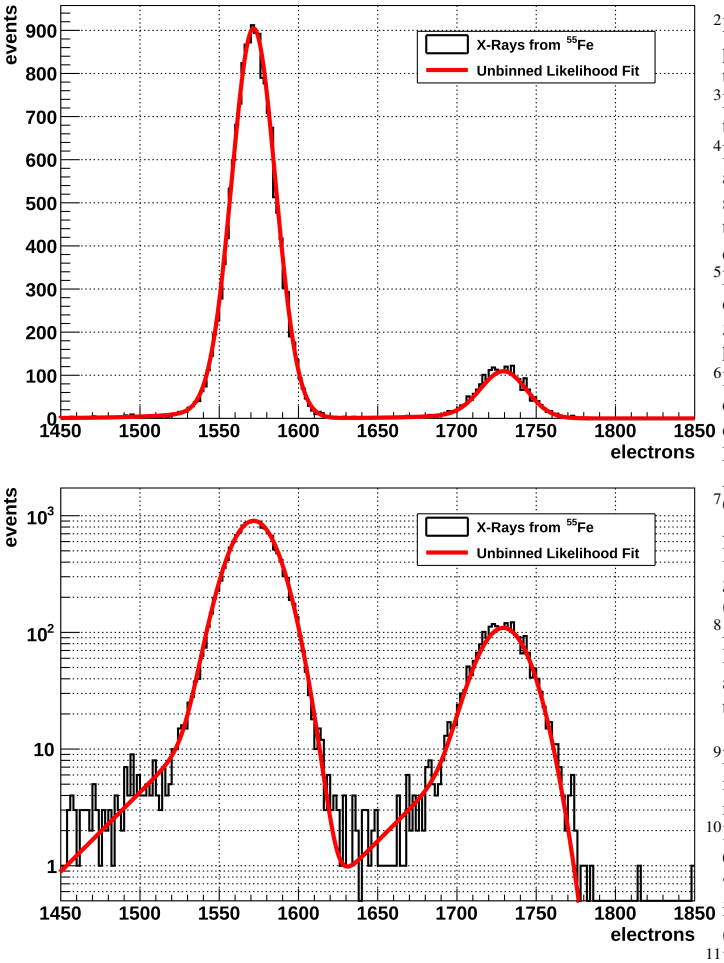

FIG. 5. X-ray peaks at 5.9 keV and 6.5 keV. Red line corresponds to the Unbinned multipeaks likelihood fit.

No. DE-AC02-07CH11359 with the U.S. Department of Energy, Office of Science, Office of High Energy Physics. The United States Government retains and the publisher, by accepting the article for publication, acknowledges that the United States Government retains a non-exclusive, paid-up, irrevocable, world-wide license to publish or reproduce the published form of this manuscript, or allow others to do so, for United States Government purposes. SU was supported in part by the Zuckerman STEM Leadership Program and DR by the National Council for Scientific and Technical Research (CONICET).

[1] U. Fano, "Ionization yield of radiations. ii. the fluctuations of the number of ions," Phys. Rev. **72**, 26–29 (1947).

[2] R. D. Ryan, "Precision measurements of the ionization energy and its temperature variation in high purity silicon radiation detectors," IEEE Transactions on Nuclear Science **20**, 473–480 (1973).

[3] R. C. Alig, "Scattering by ionization and phonon emission in semiconductors. ii. monte carlo calculations," Phys. Rev. B **27**, 968–977 (1983).

[4] P. Lechner, R. Hartmann, H. Soltau, and L. Strüder, "Pair creation energy and fano factor of silicon in the energy range of soft x-rays," Nuclear Instruments and Methods in Physics Research Section A: Accelerators, Spectrometers, Detectors and Associated Equipment **377**, 206 – 208 (1996), proceedings of the Seventh European Symposium on Semiconductor.

[5] F. Scholze, H. Rabus, and G. Ulm, "Mean energy required to produce an electron-hole pair in silicon for photons of energies between 50 and 1500 ev," Journal of Applied Physics **84**, 2926–2939 (1998), https://doi.org/10.1063/1.368398.

[6] B. Lowe and R. Sareen, "A measurement of the electron–hole pair creation energy and the fano factor in silicon for 5.9kev x-rays and their temperature dependence in the range 80–270k," Nuclear Instruments and Methods in Physics Research Section A: Accelerators, Spectrometers, Detectors and Associated Equipment **576**, 367 – 370 (2007).

[7] O. Abramoff, L. Barak, I. M. Bloch, L. Chaplinsky, M. Crisler, Dawa, A. Drlica-Wagner, R. Essig, J. Estrada, E. Etzion, and et al., "Sensei: Direct-detection constraints on sub-gev dark matter from a shallow underground run using a prototype skipper ccd," Physical Review Letters **122** (2019), 10.1103/physrevlett.122.161801.

[8] A. Aguilar-Arevalo, X. Bertou, C. Bonifazi, G. Cancelo, A. Castañeda, B. Cervantes Vergara, C. Chavez, J. C. D'Olivo, J. C. dos Anjos, J. Estrada, and et al., "Exploring low-energy neutrino physics with the coherent neutrino nucleus interaction experiment," Physical Review D **100** (2019), 10.1103/physrevd.100.092005.

[9] D. Durnford, Q. Arnaud, and G. Gerbier, "Novel approach to assess the impact of the fano factor on the sensitivity of low-mass dark matter experiments," Physical Review D **98** (2018), 10.1103/PhysRevD.98.103013.

[10] K. Ramanathan, A. Kavner, A. E. Chavarria, P. Privitera, D. Amidei, T.-L. Chou, A. Matalon, R. Thomas, J. Estrada, J. Tiffenberg, and J. Molina, "Measurement of low energy ionization signals from compton scattering in a charge-coupled device dark matter detector," Phys. Rev. D **96**, 042002 (2017).

[11] K. Ramanathan and N. A. Kurinsky, "Ionization yield in silicon for ev-scale electron-recoil processes," (2020), to be published.

[12] G. Fraser, A. Abbey, A. Holland, K. McCarthy, A. Owens, and A. Wells, "The x-ray energy response of silicon part a. theory," Nuclear Instruments and Methods in Physics Research Section A: Accelerators, Spectrometers, Detectors and Associated Equipment **350**, 368 – 378 (1994).

[13] J. Janesick, T. Elliott, R. Bredthauer, C. Chandler, and B. Burke, "Fano-Noise-Limited CCDs," in *X-Ray Instrumentation in Astronomy II*, Vol. 0982, edited by L. Golub, International Society for Optics and Photonics (SPIE, 1988) pp. 70 – 95.

[14] A. Owens, G. Fraser, and K. J. McCarthy, "On the experimental determination of the fano factor in si at soft x-ray wavelengths," Nuclear Instruments and Methods in Physics Research Section A: Accelerators, Spectrometers, Detectors and Associated Equipment **491**, 437 – 443 (2002).

[15] J. Janesick and J. Tower, "Particle and photon detection: Counting and energy measurement," Sensors **16** (2016), 10.3390/s16050688.

[16] I. Kotov, P. O'Connor, and H. Neal, "Pair creation energy and fano factor of silicon measured using fe55 x-rays," (2018) p. 51.

[17] C. Bebek, J. Emes, D. Groom, S. Haque, S. Holland, P. Jelinsky, A. Karcher, W. Kolbe, J. Lee, N. Palaio, D. Schlegel, G. Wang, R. Groulx, R. Frost, J. Estrada, and M. Bonati, "Status of the CCD development for the dark energy spectroscopic instrument," Journal of Instrumentation **12**, C04018–

C04018 (2017).

[18] J. Tiffenberg, M. Sofo-Haro, A. Drlica-Wagner, R. Essig, Y. Guardincerri, S. Holland, T. Volansky, and T.-T. Yu, "Single-Electron and Single-Photon Sensitivity with a Silicon Skipper CCD," Phys. Rev. Lett. **119**, 131802 (2017).

[19] S. E. Holland, D. E. Groom, N. P. Palaio, R. J. Stover, and Mingzhi Wei, "Fully depleted, back-illuminated charge-coupled devices fabricated on high-resistivity silicon," IEEE Transactions on Electron Devices **50**, 225–238 (2003).

[20] G. F. Moroni, F. Chierchie, M. S. Haro, L. Stefanazzi, A. Soto, E. E. Paolini, G. Cancelo, K. Treptow, N. Wilcer, T. Zmuda, J. Estrada, and J. Tiffenberg, "Low Threshold Acquisition Controller for Skipper Charge Coupled Devices," in *2019 Argentine Conference on Electronics (CAE)* (2019) pp. 86–91.

[21] G. M. Bernstein, T. M. C. Abbott, S. Desai, D. Gruen, R. A. Gruendl, M. D. Johnson, H. Lin, F. Menanteau, E. Morganson, E. Neilsen, K. Paech, A. R. Walker, W. Wester, and B. Y. and, "Instrumental response model and detrending for the dark energy camera," Publications of the Astronomical Society of the Pacific **129**, 114502 (2017).

[22] M. S. Haro, G. F. Moroni, and J. Tiffenberg, "Studies on small charge packet transport in high-resistivity fully depleted ccds," IEEE Transactions on Electron Devices , 1–8 (2020).

[23] G. Bortels and P. Collaers, "Analytical function for fitting peaks in alpha-particle spectra from si detectors," International Journal of Radiation Applications and Instrumentation. Part A. Applied Radiation and Isotopes **38**, 831 – 837 (1987).

[24] R. Pehl, F. Goulding, D. Landis, and M. Lenzlinger, "Accurate determination of the ionization energy in semiconductor detectors," Nuclear Instruments and Methods **59**, 45 – 55 (1968).

[25] K. J. McCarthy, A. Owens, A. Holland, and A. A. Wells, "Modelling the x-ray response of charge coupled devices," Nuclear Instruments and Methods in Physics Research Section A: Accelerators, Spectrometers, Detectors and Associated Equipment **362**, 538 – 546 (1995).

[26] M. Mazziotta, "Electron–hole pair creation energy and fano factor temperature dependence in silicon," Nuclear Instruments and Methods in Physics Research Section A: Accelerators, Spectrometers, Detectors and Associated Equipment **584**, 436 – 439 (2008).